Comparative experimental study of the mirror $^{13}N+^{12}C$ and $^{13}C+^{12}C$ elastic scatterings

E. Liénard,[1] D. Baye,[2] Th. Delbar,[1] P. Descouvemont,[2] P. Duhamel,[3] W. Galster,[1] M. Kurokawa,[4] P. Leleux,[1] I. Licot,[1] P. Lipnik,[1] C. Michotte,[1] T. Motobayashi,[4] A. Ninane,[1] J. Vanhorenbeeck,[3] and J. Vervier[1]

[1] *Institut de Physique Nucléaire, Université Catholique de Louvain, B 1348 Louvain-la-Neuve, Belgium*

[2] *Physique Nucléaire Théorique et Physique Mathématique, C.P. 229, Université Libre de Bruxelles, B 1050 Brussels, Belgium*

[3] *Institut d'Astronomie et d'Astrophysique, C.P. 226, Université Libre de Bruxelles, B 1050 Brussels, Belgium*

[4] *Department of Physics, Rikkyo University, Toshima, Tokyo 171, Japan*

(Received 12 December 1994)

The $^{13}N+^{12}C$ and $^{13}C+^{12}C$ elastic cross sections are measured at the center-of-mass energies of 7.8, 9.6, and 14.2 MeV, using radioactive ^{13}N and stable ^{13}C beams and position-sensitive solid-state detectors. These data are analyzed with the optical model assuming the same real central part of the nuclear potential for both systems as suggested by charge symmetry. The $^{13}N+^{12}C$ angular distributions display a significant backward rise which arises from a parity dependence of the nucleus-nucleus interaction, as for the mirror $^{13}C+^{12}C$ system. The corresponding parity terms in both potentials are similar when the different charges of the exchanged nucleons and their different binding energies are properly taken into account. A smaller imaginary part is obtained for $^{13}N+^{12}C$ than for $^{13}C+^{12}C$, which might be due to a smaller number of open two-body inelastic and direct reaction channels.

PACS number(s): 25.70.Bc, 24.10.Ht, 24.80.Dc

I. INTRODUCTION

Charge symmetry is a well established property of the nuclear interaction. Its effects are most easily observed in spectroscopic properties of mirror nuclei where Coulomb effects are not too important. The experimental level schemes clearly and simply display this symmetry of the strong interaction if the Coulomb energy shift is taken into account. On the other hand, the effects of charge symmetry in collisions are less obvious because there is no easy way of separating the contribution of the Coulomb force.

Various attempts to test charge symmetry in collisions between nucleons and light nuclei have sometimes led to controversy (see Ref. [1] for a review). They mainly involve the $^3H(p,\gamma)^4He$ and $^3He(n,\gamma)^4He$ reactions and the reversed photonuclear reactions. The most recent data and calculations on these reactions do not indicate a significant charge-symmetry violation [2]. Charge symmetry is also well tested by the Barshay-Temmer theorem [3] in transfer reactions where the colliding nuclei have zero isospins and the exit channel consists of a pair of mirror nuclei. Such studies can be performed by colliding stable nuclei [4].

Except with the $^3H/^3He$ pair, charge symmetry cannot easily be studied in elastic scatterings of mirror systems because, for mass numbers A larger than 7, all pairs of mirror nuclei contain a short-lived nucleus. With the advent of radioactive nuclear beams [5,6], it becomes possible to study mirror elastic collisions involving heavy ions. Charge symmetry must introduce some relationship between these reactions but no simple recipe exists for relating their cross sections. Indeed, the complexity of the interpretation of cross sections increases considerably with increasing A. The Coulomb force which dominates the collision process below the Coulomb barrier is much stronger than for very light systems. The existence of many open channels (whose threshold energy is also sensitive to Coulomb effects) may completely hide the manifestations of charge symmetry above this barrier.

In the present paper, we address the problem of relating mirror elastic collisions between heavy ions in a simultaneous study of the $^{13}N+^{12}C$ and $^{13}C+^{12}C$ systems. The postaccelerated ^{13}N radioactive beam at the Louvain-la-Neuve facility allows us to study the $^{13}N+^{12}C$ reaction. Experiments were carried out at three laboratory energies: 16.3, 20.0, and 29.5 MeV. In the center-of-mass (c.m.) frame these energies correspond to 7.8, 9.6, and 14.2 MeV, respectively, covering an energy range from just above to about twice the Coulomb barrier. The mirror $^{13}C+^{12}C$ scattering is very well documented [7–9] and switching from the radioactive ^{13}N beam to the stable ^{13}C beam allows us to check the reliability of the present results. The cross sections are obtained from 14° to about 150° in the c.m. frame. In the same experiment, data on the $^{13}N+^{13}C$ and $^{13}C+^{13}C$ elastic scatterings were taken with the same setup, except for the target [10]. These results and their analysis will be reported elsewhere.

The $^{13}N+^{12}C$ and $^{13}C+^{12}C$ elastic cross sections are analyzed simultaneously with the potential model. Charge symmetry implies that the real central parts of

both optical potentials should be very similar, except for the known Coulomb interactions and for the parity effect discussed below. On the other hand, the imaginary parts might be different since the absorption into direct channels depends on the thresholds of the different inelastic and reaction channels. With about 10^8 particles per second in the radioactive beam, a direct fit of our limited $^{13}N+^{12}C$ data with an optical potential is not expected to test charge symmetry in an accurate way. In order to bypass this difficulty, instead of testing charge symmetry, we choose to perform a theoretical analysis which adopts this symmetry *a priori*. We therefore assume that, except for the Coulomb and parity terms, the real parts of the mirror nucleus-nucleus potentials are identical and we perform an analysis of the $^{13}N+^{12}C$ elastic-scattering data with a potential inspired by an analysis of more extensive $^{13}C+^{12}C$ data. We employ here the simplest assumption consistent with charge symmetry. This assumption reduces the number of adjustable parameters in the $^{13}N+^{12}C$ case and removes ambiguities from the fitting procedure. Results found with this method, if satisfactory, will provide a first confirmation of the validity of charge symmetry in mirror elastic collisions between heavy ions, since most parameters of the $^{13}N+^{12}C$ potential are deduced from the $^{13}C+^{12}C$ interaction.

In order to correctly study charge symmetry with the $^{13}N+^{12}C$ and $^{13}C+^{12}C$ collisions, an important characteristic of these systems has to be taken into account. During the collision process, the valence nucleon can be transferred — or equivalently the identical ^{12}C cores can be exchanged — and the corresponding amplitude contributes to elastic scattering [8,11,12]. This effect gives rise to a parity dependence in the nucleus-nucleus potential, i.e., the same potential cannot be used for even and for odd partial waves. Such a parity dependence can be understood microscopically as arising from the combined effects of Pauli antisymmetrization with respect to all the nucleons involved in the collision process, and of parity conservation [13–15]. The parity effect is especially strong when the mass-number difference is 1 [13,16]. The parity term is sensitive to the asymptotic behavior of the valence-nucleon wave function with respect to the ^{12}C core [8]. Hence this term depends predominantly on the binding energy E_B of this nucleon. Because of Coulomb effects, this energy is very different in ^{13}C ($E_B = 4.946$ MeV) and in ^{13}N ($E_B = 1.944$ MeV). Moreover, the transfer of a proton is not identical to the transfer of a neutron since the tail of its bound-state wave function is affected by the Coulomb interaction. Therefore the parity terms differ in mirror collisions and may contribute to hide charge symmetry. However, the form factor of this term is well understood in $^{13}C+^{12}C$ and the measurement of $^{13}N+^{12}C$ elastic-scattering cross sections offers a unique opportunity of analyzing it in the mirror case.

The experimental setup and the results are described in Sec. II. An optical-model study of these data is performed in Sec. III. For the parity dependence in $^{13}N+^{12}C$ scattering, we generalize the physical picture which has been found to be efficient for $^{13}C+^{12}C$. The properties of the resulting potential are discussed in Sec. IV. Concluding remarks are presented in Sec. V.

II. EXPERIMENTAL PROCEDURE

A. Setup

The ^{13}N radioactive beam of Louvain-la-Neuve is obtained by a two-cyclotron scheme described in detail elsewhere [6]. $^{13}N^{2+}$ beams are postaccelerated to energies of 16.3, 20.0, and 29.5 MeV, with intensities up to about 1.2×10^8 particles/s, and sent to a 1 m diameter reaction chamber. The ^{12}C and ^{13}C self-supporting targets, 40 $\mu g/cm^2$ thick, were produced by evaporation in Louvain-la-Neuve and Erlangen, respectively.

Two passivated implanted planar silicon (PIPS) detectors placed at $+15°$ and $-15°$ with respect to the beam axis monitor the incoming angle of the incident beam. They are collimated to 2 mm × 6 mm and are at a distance of 48 cm from the target. Two large ion-implanted silicon detectors [17] register the elastically scattered ^{13}N or ^{13}C ions, or the recoiling ions from the carbon targets. Each detector is made of 12 resistive strips, 60 mm long and 5 mm wide, separated vertically by a gap of 50 μm. The signals from both ends of each strip allow the determination of the particle energy and of its position along the strip. The detectors are located on a rotatable plateau at mean distances of 20 and 25 cm from the target and the angle between their mean position is 22°. In this way, the angular distributions of the $^{13}N+^{12}C$ and $^{13}C+^{12}C$ elastic scattering are obtained from 15° to 150° in the c.m. system with only two different angle settings.

The energy calibration of the detectors is obtained by ^{13}C + Au elastic scattering and by means of a ^{241}Am α source. The calibration in position along the strips is performed by placing a grid with seven vertical slits in front of the detectors.

The 24 signals coming from the strips of each multistrip detector are fed into preamplifiers (under vacuum) and shaping amplifiers. Analog-to-digital converter modules are gated by a common signal generated by the backplane of the detector. The data acquisition is controlled by a personal computer, reading data from a CAMAC crate. The data are sent by a VME processor to a magnetic tape and simultaneously transferred to a monitoring task.

Downstream of the main setup, a possible ^{13}C contamination of the ^{13}N beam is monitored on line by scattering the outgoing beam on a gold foil, the scattered ^{13}C and ^{13}N ions being detected at 25°. A 1 mg/cm^2 thick aluminum degrader foil is placed in front of all the detectors in order to achieve a clear separation between C and N ions, taking advantage of the different stopping powers of those ions.

Ten days of data acquisition were needed to measure, at three energies, the angular distributions for the elastic scatterings of the ^{13}C and ^{13}N beams on ^{12}C and ^{13}C targets. The data with the ^{13}C beam are mainly used to check the consistency with existing data [9,18].

The angular offset of the detectors with respect to the real beam axis is determined by fitting data at small angles ($\theta < 20°$) to Rutherford scattering or, at 14.2 MeV, to results of the optical model as discussed below. Around 45° in the laboratory, we check that the same cross sections are obtained by detecting either the

mass-13 or the mass-12 ions in the $^{13}C+^{12}C$ or $^{13}N+^{12}C$ systems. The angular offset is found to be at most 1°.

B. Results

The $^{13}N+^{12}C$ angular distributions are determined from the scattered ^{13}N and recoil ^{12}C ions. The former provide the data points between 15° and about 100° in the c.m. system, while the latter give the data between about 80° and 150°. The energies of the ^{12}C peaks, whose intensity is much weaker than those of the ^{13}N peaks, are imposed by the high-statistics data taken in the $^{13}C+^{12}C$ scattering at the same incident energy. Figure 1 shows experimental spectra of the two mirror scatterings measured at an energy of 20 MeV and at a mean angle of 26° in the laboratory frame. Each peak is fitted by a Gaussian distribution with an exponential tail taking into account the imperfect charge collection in the detector. The peaks are superimposed on a linear background. A global χ^2 fit of the energy spectrum is performed, at each angle, using the MINUIT minimization code [19]. In the upper spectrum of Fig. 1, the ^{12}C recoil ions are strongly

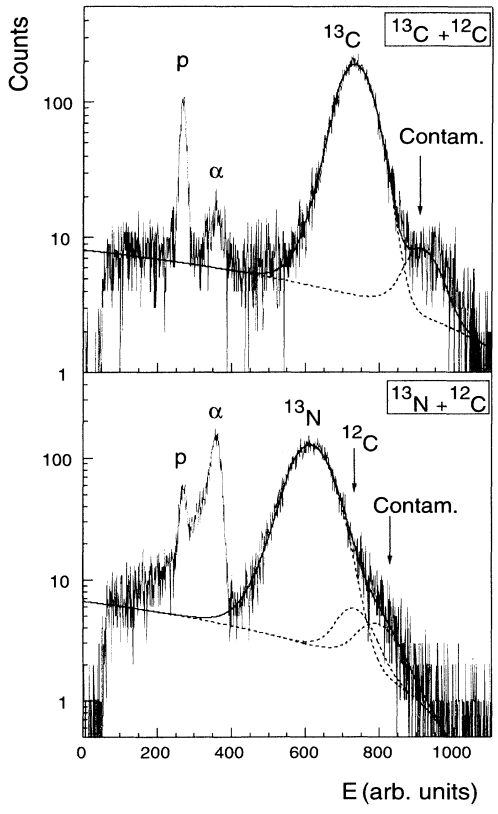

FIG. 1. Experimental spectra of $^{13}C+^{12}C$ and $^{13}N+^{12}C$ elastic scatterings at 9.6 MeV in the c.m. frame and at a mean laboratory angle of 26°. The energy E is in arbitrary units. The different peaks are explained in the text. The solid lines show global fits of the spectra, with the contribution of each peak (dotted lines).

mixed with the ^{13}C scattered ions because of the poor energy resolution and the very small kinematical separation at this small angle. However, the contribution of ^{12}C is very small compared with ^{13}C in the $^{13}C+^{12}C$ spectrum. Hence, the single ^{13}C peak imposes the shape and position of the ^{12}C curve in the $^{13}N+^{12}C$ spectrum (lower part of Fig. 1). The proton peak comes probably from the beam scattering on water present in the target, and the α particles come from the ^{241}Am calibration source. The last peak (denoted as "Contam." in Fig. 1) is due to a heavy contaminant present in the target, as discussed later on.

As a test of the MINUIT routine, we simulated a spectrum similar to the observed ones: we generated two Gaussian peaks with a width and an energy separation typical of the data, and a ratio of amplitudes equal to 0.02. This spectrum was analyzed by MINUIT with the constraints of keeping identical widths and a fixed centroid for the small peak. The program was able to retrieve the original parameters. The integrals of the peaks were exact at the level of 2.5 %, which is half the statistical uncertainty reported by the program. When the position of the small peak that simulated the ^{12}C recoils was changed within reasonable limits corresponding to the experimental uncertainties, the integral of the peaks varied by an amount less than the uncertainty reported by the fitting routine. Hence, this latter value was adopted.

Each data point of the angular distributions is an average cross section within an angular interval of 1° in the laboratory frame. The absolute normalization is obtained by equating to unity its ratio to the Rutherford cross section (σ/σ_R) at very small angles. This procedure is in agreement with the value 1 obtained with the optical potential described in the next section, for the two lower energies. At a c.m. energy of 14.2 MeV, the predicted value of the same ratio at a c.m. angle of 20° is 1.10 for $^{13}C+^{12}C$ and 1.14 for $^{13}N+^{12}C$. This value does not change by more than 5% with different potential parameters. Hence the experimental data are normalized by equating the first three data points to the optical-model values.

The two different locations of the detectors, necessary to cover the whole angular distribution up to 150° c.m., are linked by an angular overlap in order to normalize the two sets of data to each other. In such a way, the normalization is independent of experimental conditions such as beam intensity and target thickness, thereby minimizing systematic errors.

Finally, two corrections are applied to the data. First, the elastic scattering of ^{13}N (^{13}C) on the ^{16}O and W contaminants (Fig. 1) is subtracted from the data of interest in the regions where the kinematical curves overlap; the tungsten comes from the filament used to evaporate the targets (these corrections are not applied to the data presented in Ref. [10]; this explains the small differences which can be observed). Second, a contribution due to the ^{13}C contamination of the ^{13}N radioactive beam is also estimated: considering all the runs, the $^{13}C/^{13}N$ ratio reaches an average value of about 0.2%. The corresponding correction, computed from the $^{13}C+^{12}C$ data, is subtracted from the backscattered peaks, assumed to be

mixed with the ^{13}C contaminant. The effect depends on the relative behavior of the angular distributions. It becomes significant at large angles around 140°–150° c.m. At 20 MeV, for example, the contamination represents 35% (±12%) of the recoil peak which yields the cross section at 146° in the c.m. frame.

Our ^{13}C+^{12}C elastic-scattering data at 7.8 MeV (see Fig. 2 in the next section) are in agreement with the data in the literature [9]. The method used to separate the recoil nuclei from the scattered ones limits all the curves to a maximum angle of about 150°. The ^{13}N+^{12}C elastic-scattering data are presented below in Fig. 3. The last two angular distributions are incomplete around 90° due to poor statistics.

III. POTENTIAL-MODEL ANALYSIS OF ANGULAR DISTRIBUTIONS

The nuclei involved in both reactions differ by only one nucleon. In the elastic-transfer model [8,11], two scattering amplitudes corresponding to the direct scattering and the elastic transfer of the valence nucleon appear and their interference induces the observed structures in the angular distributions of elastic cross sections. In a microscopic model, where all the nucleons are taken into account, direct and transfer amplitudes do not appear separately; nevertheless, the indiscernibility of the nucleons and the Pauli principle are responsible for the occurrence of a parity term in the potential which leads to the same physical consequences [13]. The dominant component of the parity effect is due to the simultaneous exchange of all the core nucleons. This provides a microscopic foundation for the elastic-transfer model. The parity effect, which should occur in many cases of elastic collisions between heavy ions [14], is especially strong when a single nucleon is transferred.

A parity dependence is well described in the optical model when a central nuclear potential V_N is complemented by a parity term V_p as [14]

$$V = V_N + (-1)^l V_p \tag{1}$$

where l is the orbital momentum of the relative motion. The parity form factor V_p can be positive or negative, depending on the nuclei involved in the collision. Its sign determines which among the even-wave potential $V_N + V_p$ and the odd-wave potential $V_N - V_p$ is deeper. A simple rule derived from the microscopic model predicts the parity of the deeper potential [14]

$$(-1)^l = \begin{cases} (-1)^{A<} & (s \text{ shell}, sd \text{ shell}) \\ (-1)^{A>} & (p \text{ shell}, pf \text{ shell}) \end{cases} \tag{2}$$

where $A_<$ and $A_>$ correspond, respectively, to the smaller and larger mass numbers among the scattered nuclei. In the present case, the ^{13}N (or ^{13}C) and ^{12}C nuclei belong to the p shell and the potential V should be deeper for odd waves than for even waves, i.e., V_p should be positive.

The total potential V of Eq. (1) is used in an optical-model formalism to fit the data. Energy-independent Saxon-Woods form factors are chosen for the real (R) and imaginary (I) parts of the nuclear potential

$$V_N(r) = V f_R(r) + iW f_I(r) \tag{3}$$

where

$$f_j(r) = \left(1 + \exp \frac{r - R_j}{a_j}\right)^{-1} \tag{4}$$

with $j = R$ or I. For simplicity, we do not introduce any energy dependence in the parameters. Tests have shown that such dependences cannot significantly be extracted from the present sets of data, because both of their limited energy range and their limited accuracy. The Coulomb potential is described by a sphere-sphere approximation with $r_c = 1.74$ fm [20].

The expression of the parity term V_p should be derived from microscopic models. However, in order to treat the c.m. motion exactly, these models are until now based on harmonic-oscillator orbitals for which the tail of the parity term presents an unrealistic Gaussian behavior [14]. When a single neutron is exchanged, von Oertzen [8] has shown that a simple expression can be derived for V_p from the theory of Buttle and Goldfarb [21] in the case of the ^{13}C+^{12}C system. Let us define the wave number of the transferred nucleon in the core potential

$$\kappa = (2\mu E_B/\hbar^2)^{1/2} \tag{5}$$

and its Sommerfeld parameter

$$\eta = \frac{Ze^2}{\hbar(2E_B/\mu)^{1/2}} \tag{6}$$

where E_B is the binding energy of the valence nucleon, Ze is the core charge, and μ is the reduced mass of the core-nucleon system. According to Ref. [8], the parity potential resembles the asymptotic form of the valence neutron wave function in the potential of the ^{12}C core, and reads

$$V_p(^{13}\text{C}+^{12}\text{C}) = F_n c(0, \kappa_n r) \exp(-\kappa_n r)/\kappa_n r \tag{7}$$

where $\kappa_n = 0.469$ fm^{-1}, F_n is an adjustable amplitude, and the cutoff factor c is defined below. This parity potential is purely real. Some authors have considered the possibility of a parity-dependent imaginary part (see references in Ref. [11]) but the physical origin of such a term is completely different from the Pauli effects that we discuss here. Its shape would therefore be very different from the shape of V_p in Eq. (7). In particular, it will not exhibit the slow decrease which leads to a longer range for V_p than for V_N and which makes the effect of V_p so important.

For the mirror ^{13}N+^{12}C reaction, the Coulomb interaction between the core and the valence proton complicates the situation. We show in the Appendix that in that case the parity term V_p is also given, to a good approximation, by the asymptotic form of the proton wave function. However, the expression (A5) contains a Whittaker function which is rather complicated for a potential model. In order to keep rather simple form factors in the potentials, we choose to replace the Whittaker function by its

asymptotic form. The parity term is then expressed as

$$V_p(^{13}\mathrm{N}+^{12}\mathrm{C}) = F_p c(\eta, \kappa_p r) \exp(-\kappa_p r)/2^{\eta}(\kappa_p r)^{1+\eta} \quad (8)$$

where $\kappa_p = 0.294\ \mathrm{fm}^{-1}$, $\eta = 0.653$, and F_p is a parameter. The c factors appearing in (7) and (8) are cutoff functions introduced to regularize the parity terms at the origin. They are defined as

$$c(\eta, x) = 1 - \exp(-nx^{1+\eta}) \quad (9)$$

with $n = 5$ for $^{13}\mathrm{C}+^{12}\mathrm{C}$ and $n = 11$ for $^{13}\mathrm{N}+^{12}\mathrm{C}$. These values lead to similar cutoff factors for both systems. A change of the cutoff parameter n by one unit in expression (9) does not give rise to noticeable changes in the results, showing the weak sensitivity of the analysis to details of the cutoff function. When η is replaced by zero, $V_p(^{13}\mathrm{N}+^{12}\mathrm{C})$ in Eq. (8) reduces to $V_p(^{13}\mathrm{C}+^{12}\mathrm{C})$ in Eq. (7). The physical interpretation of F_n and F_p is discussed in Sec. IV.

As explained in the Introduction, in a first step, we start from a set of $^{13}\mathrm{C}+^{12}\mathrm{C}$ data, found in the literature [9] or measured in the present experiment. These data are fitted to determine the parameters of a $^{13}\mathrm{C}+^{12}\mathrm{C}$ optical potential, which contains the parity term (7). For simplicity we do not allow any energy dependence of the parameters. However, as usual, either deep or shallow potentials can be employed in the model [15]. The best results that we obtain are presented in Fig. 2 and the corresponding parameter values are listed in Table I. The quality of the fit is almost identical with both potentials which provide a reasonable reproduction of the data except around 70°–80° c.m. where some structure is missing at most energies. The backward data at 11.72 MeV are also not well reproduced. However, the quality of these fits is similar to that obtained with the distorted-wave Born approximation (DWBA) and coupled-channel formalisms [9].

In a second step, the data on the mirror $^{13}\mathrm{N}+^{12}\mathrm{C}$ system (see Fig. 3) are studied with potentials requiring minimum changes and taking into account the charge of the transferred nucleon. These changes arise in the Coulomb interaction, where the charges are adapted, and in the parity term, which is modified as indicated in Eq. (8). The depth W of the imaginary part in (3) is also varied since absorption is not supposed to comply with charge symmetry. However, the form factor of the imaginary part is not modified. As shown in Fig. 3, the agreement with the data is satisfactory for the potentials given in Table I, with the parity term given by Eq. (8). The differences between the cross sections calculated with

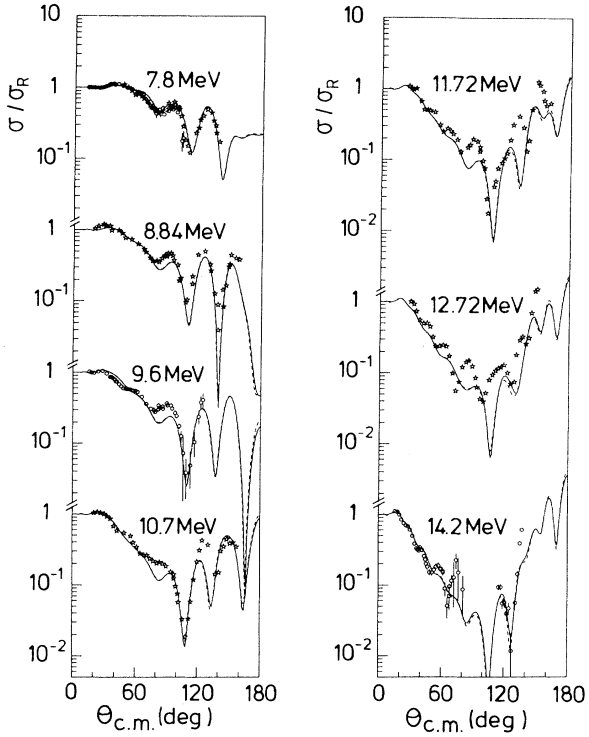

FIG. 2. Potential-model fits [Eqs. (1) and (3)–(7)] of the $^{13}\mathrm{C}+^{12}\mathrm{C}$ data of Ref. [9] (7.8, 8.84, 10.7, 11.72, and 12.72 MeV — stars) and of the present experiment (7.8, 9.6, and 14.2 MeV — dots). The dashed and solid lines correspond to the deep and shallow potentials defined in Table I, respectively.

the deep and shallow potentials are larger than in the $^{13}\mathrm{C}+^{12}\mathrm{C}$ case, especially at 14.2 MeV. However, these differences are not really significant because error bars are large in the backward region. The values of F_p are rather different for both potentials, when the three energies are taken into account. They are in closer agreement when the third energy is not included in the fit, as in the calculation performed in the next section.

The overall agreement observed for both collisions gives confidence in the parameters found and confirms the validity of charge symmetry in these analog reactions. The amplitudes of the parity terms and the differences between the imaginary terms found in this analysis are discussed in the next section.

TABLE I. Potential parameters [Eqs. (1), (3), (4), and (7) for $^{13}\mathrm{C}+^{12}\mathrm{C}$ or (8) for $^{13}\mathrm{N}+^{12}\mathrm{C}$].

		V (MeV)	R_R (fm)	a_R (fm)	W (MeV)	R_I (fm)	a_I (fm)	$F_{n,p}$ (MeV)
Shallow	$^{13}\mathrm{C}+^{12}\mathrm{C}$	−16.6	5.92	0.56	−17.3	5.87	0.44	26.6
	$^{13}\mathrm{N}+^{12}\mathrm{C}$				−3.0			9.9
Deep	$^{13}\mathrm{C}+^{12}\mathrm{C}$	−115.8	5.05	0.50	−22.1	5.05	0.51	26.5
	$^{13}\mathrm{N}+^{12}\mathrm{C}$				−8.6			13.0

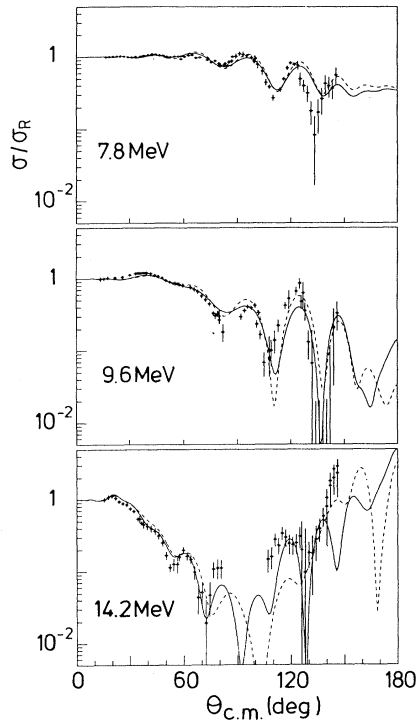

FIG. 3. Ratios of ^{13}N+^{12}C elastic cross sections to Rutherford cross sections, measured at 7.8, 9.6, and 14.2 MeV in the c.m. frame. Comparison with potential-model fits of the ^{13}N+^{12}C data, calculated with the parity potential of Eq. (8) taking account of the charge of the transferred nucleon. The dashed and solid lines correspond to the deep and shallow potentials defined in Table I, respectively.

IV. COMPARISON BETWEEN THE MIRROR POTENTIALS

The good agreement between the data and the optical model justifies the use of the real part of the ^{13}C+^{12}C potential for the ^{13}N+^{12}C system. We can therefore analyze the differences between the two potentials given in Table I on physical grounds. Let us start with the parity terms.

The parity terms are obviously not identical. This is easily understood when one realizes that all the differences are related to Coulomb effects. Indeed the Coulomb repulsion reduces the binding of the proton in ^{13}N and distorts its wave function. However, the two parity terms present similarities. First they have the same sign: F_n and F_p are both positive. This is to be expected as the sign of V_p is a consequence of the Pauli principle, which acts in a similar way in mirror systems [14]. This sign is in agreement with the simple rule (2).

A second similarity appears in the physical interpretation of the parameters F_n and F_p. Their values displayed in Table I weakly depend on the deep or shallow nature of the potential. The parameter F_n appearing in (7) can be factorized as [8]

$$F_n = S_n N_n^2 \frac{\hbar^2 \kappa_n}{2\mu} \tag{10}$$

where S_n is the spectroscopic factor for the valence neutron in ^{13}C. The asymptotic normalization constant N_n of the neutron orbital follows the definition of Ref. [22] [see also Eq. (A2) in the Appendix]. With $V_0 = 45.7$ MeV, the ^{12}C $+n$ potential of Gubler *et al.* [22] provides the value $N_n = 1.72$ fm$^{-1/2}$. From Table I, we derive $S_n = 0.85$ in good agreement with the value 0.81 ± 0.04 derived in Ref. [22]. Conversely, the latter value could be used to reduce the number of free parameters in the fit of the ^{13}C+^{12}C data.

Understanding the constant F_p requires more caution. Indeed, in (8), we have chosen a simplified form for the parity potential, in order to avoid the use of the Whittaker function $W_{-\eta,1/2}(2\kappa r)$. This function is about 20% smaller than its asymptotic approximation $\exp(-\kappa r)/(2\kappa r)^\eta$ between 5 and 8 fm, so that F_p has to be rescaled. Here we prefer to consider a regularized version of (A5),

$$\hat{V}_p(^{13}\mathrm{N}+^{12}\mathrm{C}) = \hat{F}_p c(0, \kappa_p r) W_{-\eta,1/2}(2\kappa_p r)/\kappa_p r, \tag{11}$$

which inspires the approximation (8). In this expression, the strength is given by

$$\hat{F}_p = S_p N_p^2 \frac{\hbar^2 \kappa_p^2}{2\mu\kappa_{\mathrm{eff}}} \mathcal{N} \tag{12}$$

where $\kappa_{\mathrm{eff}} = 0.357$ fm^{-1} and $\mathcal{N} = 0.625$ are determined from Eq. (A3). The constant $N_p = 1.85$ fm$^{-1/2}$ is calculated with a ^{12}C $+ p$ potential derived from the ^{12}C $+ n$ potential of Ref. [22] modified by a Coulomb term and by a slightly readjusted depth ($V_0 = 44.5$ MeV), which fits the binding energy of the proton. At 7.8 MeV, the effects of the central part of the nuclear potential are minimum because we are close to the Coulomb barrier (7.3 MeV). When we fit $\hat{F}_p$ at this energy with the potential defined by (1) and (11), we obtain values close to 11.8 MeV for the deep and shallow potentials. This corresponds to a spectroscopic factor close to unity. The accuracy of this result cannot easily be evaluated because the error bars reduce the sensitivity to $\hat{F}_p$, but the mere fact that the value of S_p is physically plausible also corroborates the validity of the present analysis. Within the uncertainty on S_p this result is also compatible with charge symmetry. At distances where the parity term plays an important role, $W_{-\eta,1/2}$ is equal to about 80% of its asymptotic approximation, so that a ratio $F_p/\hat{F}_p \approx 0.8$ is expected. This is verified in Table I by the value of F_p for the shallow potential, but not for the deep one. However, let us recall here that F_p results from a global fit of the three energies, while $\hat{F}_p$ is fitted at 7.8 MeV only.

In order to reduce the number of parameters in the potential, a first approximation for $\hat{F}_p$ can be obtained by assuming $S_p = S_n$. This charge-symmetry assumption for S_p is compatible with the scattered values encountered in the literature. They range from 0.38 to 1.48, with the latest results below S_n (see reviews in Refs. [23,24]).

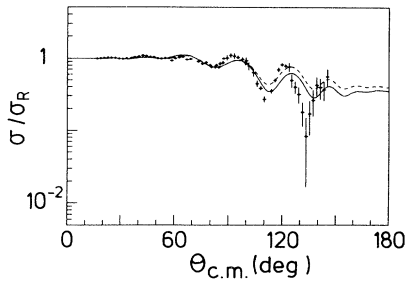

FIG. 4. Comparison of the experimental $^{13}N+^{12}C$ angular distribution at 7.8 MeV with a calculation using the parity potential defined in Eq. (11) involving the amplitude $\hat{F}_p$ [Eq. (12)] computed with the ^{13}C spectroscopic factor $S_n = 0.81$. The dashed and solid lines correspond to the deep and shallow potentials, respectively.

The choice $S_p = 0.81$ provides the value $\hat{F}_p = 9.4$ MeV. The obtained parity potential $\hat{V}_p$ is tested in Fig. 4 with respect to the data. One observes that the quality of the results is very close to that obtained in Fig. 3. An approximation for F_p is given by $0.8\hat{F}_p$. We can conclude that the parity term for $^{13}N+^{12}C$ can also be derived from the corresponding term in $^{13}C+^{12}C$, at least within the accuracy of the present data.

Finally, Table I shows that the strength W of the imaginary term is reduced in $^{13}N+^{12}C$ scattering with respect to $^{13}C+^{12}C$, independently of the deep or shallow nature of the real term. Some previous $^{13}C+^{12}C$ potentials [11] display a smaller imaginary part but they only concern energies close to the barrier. When the full sets of $^{13}C+^{12}C$ and $^{13}N+^{12}C$ data are fitted, a larger value of W is obtained for the former system. The sensitivity with respect to W is illustrated in Fig. 5 for the shallow potential at our highest energy, i.e., 14.2 MeV. We present

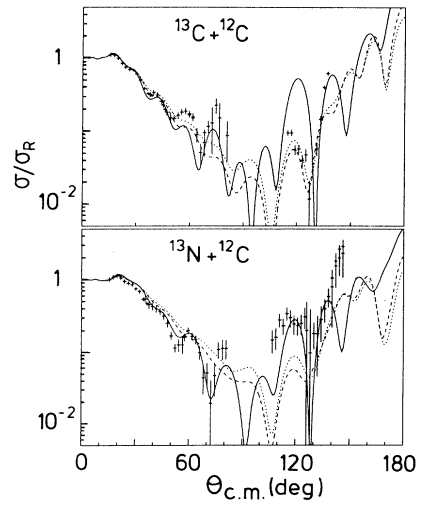

FIG. 5. Sensitivity with respect to W of the $^{13}C+^{12}C$ and $^{13}N+^{12}C$ shallow potentials, at 14.2 MeV. The solid, dashed, and dotted lines correspond to $W = -3$, -10, and -17 MeV, respectively.

results for three W values, either typical of one system or intermediate. The differences between W values for $^{13}C+^{12}C$ and $^{13}N+^{12}C$ correspond to differences in behaviors at back angles, with a more important rise for the $^{13}N+^{12}C$ σ/σ_R ratio. This effect may to some extent be due to the higher Coulomb barrier of the $^{13}N+^{12}C$ system. The barrier increase should play a role at low energies but cannot completely explain the strong reduction of W. A more important cause for this reduction is the fact that ^{13}N is more fragile than ^{13}C: it has no bound excited state. The number of *two-body* channels available for the absorption into direct channels (inelastic and reaction channels) is smaller for $^{13}N+^{12}C$ scattering. Since two-body channels provide the most efficient absorption at angular momenta close to the grazing value, this reduction should explain the weaker value of W for $^{13}N+^{12}C$ [25]. When other data on pairs of mirror heavy-ion systems become available, it will be interesting to explore the generality of this phenomenon.

V. CONCLUSION

We have measured the $^{13}N+^{12}C$ and $^{13}C+^{12}C$ elastic scatterings with the same experimental setup at three energies over a large angular range. The present experimental data offer a first opportunity of considering the effects of charge symmetry in mirror elastic collisions between heavy ions. Simultaneously these data provide a new insight into the study of parity dependence in heavy-ion scattering. They will also allow further tests of other models such as coupled-channel descriptions of heavy-ion reactions [12].

We first fit the more detailed $^{13}C+^{12}C$ data with energy-independent potentials. Then, because of charge symmetry, we assume that the real part of the $^{13}N+^{12}C$ nucleus-nucleus potential is the same as for the $^{13}C+^{12}C$ system, except for the known Coulomb and parity terms. In addition, we keep the same form factor for the imaginary part. Therefore only two parameters of the $^{13}N+^{12}C$ potential remain to be adjusted, i.e., the strengths of the imaginary and parity terms. The quality of the final results supports this interpretation of charge symmetry. A simple formalism is thus able to reproduce consistently the scattering cross sections of two mirror systems of heavy ions.

When a proton is transferred, the usual parity term, which is valid for the elastic transfer of a neutron [8], must be generalized. Satisfactory results are provided by a natural extension which takes the charge of the transferred nucleon into account. The sign of the parity term is the same for both mirror systems in agreement with the simple rule (2).

The spectroscopic factors derived from the parity term for the proton in ^{13}N and for the neutron in ^{13}C are not very different from each other, and are also compatible with charge symmetry. In fact, assuming that they are equal allows one to reduce the number of unknown parameters in the $^{13}N+^{12}C$ case to 1, i.e., the strength W of the imaginary part.

The strength W is found to be weaker for $^{13}N+^{12}C$ than for $^{13}C+^{12}C$. This effect seems physically reasonable, because the absorption into direct reaction channels should be weaker when the number of open two-body channels is smaller. However, at present, we cannot explain it quantitatively. Further studies of mirror systems will be necessary in order to learn how to transpose the known optical potential of a collision between stable nuclei into a potential valid for the mirror collision involving a radioactive nucleus.

ACKNOWLEDGMENTS

We would like to thank Professor W. von Oertzen for helpful discussions. We also are grateful to the cyclotron staff, to P. Demaret (Louvain-la-Neuve) and to M. Schmitt (Erlangen) for preparing the targets, and to H. Murakami (Rikkyo) for help with the detector electronics. Three of us, P. Descouvemont, P. Leleux, and J. Vanhorenbeeck, acknowledge financial support from the National Fund for Scientific Research, Belgium. This text presents research results of the Belgian program on interuniversity attraction poles initiated by the Belgian Federal Services for Scientific, Technical, and Cultural Affairs. Some travel expenses are supported in part by the Joint Research of Monbusho International Scientific Research Program under the Program No. 06044205.

APPENDIX

For a distance r between the colliding nuclei, we approximate the parity term with the exchange integral [8]

$$J(r) = S \int \psi^*(\boldsymbol{r}_2) V(\boldsymbol{r}_1) \psi(\boldsymbol{r}_1) d\boldsymbol{r}_1 \qquad \text{(A1)}$$

where the nucleon coordinates $\boldsymbol{r}_1$ and $\boldsymbol{r}_2$ with respect to both cores are related by $\boldsymbol{r}_2 = \boldsymbol{r} - \boldsymbol{r}_1$. In this expression S is the spectroscopic factor and ψ is the individual orbital of the valence nucleon with respect to one of the identical cores. The integral is evaluated by replacing ψ by its asymptotic form

$$\psi(\boldsymbol{r}) \to N Y_l^m(\Omega) W_{-\eta,l+1/2}(2\kappa r)/r \qquad \text{(A2)}$$

where $W_{-\eta,l+1/2}$ is a Whittaker function and N is the asymptotic normalization coefficient. When the valence particle is neutral, the radial function reduces to the Hankel function $h_l^{(1)}(\kappa r)$, and $J(r)$ is provided in Ref. [21]. However, in the proton case, no simple form is available for this integral.

In order to calculate (A1) in the proton case to a reasonable accuracy, but with a simple expression, we employ the approximation [26]

$$W_{-\eta,l+1/2}(2\kappa r)/\kappa r \approx \mathcal{N} h_l^{(1)}(\kappa_{\text{eff}} r) \ . \qquad \text{(A3)}$$

The constants $\mathcal{N}$ and κ_{eff} are parameters which can easily be fitted in each particular case. They depend on κ and η but almost not on l. This property is used below. With the approximation (A3), $J(r)$ can be calculated with the standard technique as

$$J(r) \approx S N^2 \frac{\hbar^2 \kappa^2}{2\mu\kappa_{\text{eff}}} \mathcal{N}^2 h_0^{(1)}(\kappa_{\text{eff}} r) \qquad \text{(A4)}$$

where we assume as usual that $l = 0$ dominates. Hence, reversing (A3) provides

$$J(r) \approx \hat{F} W_{-\eta,1/2}(2\kappa r)/\kappa r \qquad \text{(A5)}$$

with $\hat{F}$ given by (12). In the neutron case, $\eta = 0$, $\mathcal{N} = 1$, and $\kappa_{\text{eff}} = \kappa$, so that the traditional $J(r)$ involving (10) is recovered.

[1] D.R. Tilley, H.R. Weller, and G.M. Hale, Nucl. Phys. **A541**, 1 (1992).
[2] R.E.J. Florizone, J. Asai, G. Feldman, E.L. Hallin, D.M. Skopik, J.M. Vogt, R.C. Haight, and S.M. Sterbenz, Phys. Rev. Lett. **72**, 3476 (1994).
[3] G.M. Temmer, in *Proceedings of the International Course on Fundamentals in Nuclear Theory*, Trieste, 1966, edited by A. de Shalit and C. Villi (IAEA, Vienna, 1967), p. 163.
[4] W. von Oertzen, J.C. Jacmart, M. Liu, F. Pougheon, J.C. Roynette, and M. Riou, Phys. Lett. **28B**, 482 (1969).
[5] *Proceedings of the Second International Conference on Radioactive Nuclear Beams*, Louvain-la-Neuve, 1991, edited by Th. Delbar (Adam-Hilger, Bristol, 1992); *Proceedings of the Third International Conference on Radioactive Nuclear Beams*, East Lansing, 1993, edited by D.J. Morrissey (Frontières, Gif-sur-Yvette, 1993).
[6] P. Van Duppen, P. Decrock, M. Huyse, Th. Delbar, W. Galster, P. Leleux, I. Licot, E. Liénard, P. Lipnik, M. Loiselet, C. Michotte, G. Ryckewaert, J. Vervier, P. Duhamel, and J. Vanhorenbeeck, Nucl. Instrum. Methods Phys. Res. Sect. B **70**, 393 (1992); Nucl. Phys. **A553**, 837c (1993).
[7] A. Gobbi, U. Matter, J.L. Perrenoud, and P. Marmier, Nucl. Phys. **A112**, 537 (1968).
[8] W. von Oertzen, Nucl. Phys. **A148**, 529 (1970).
[9] H. Voit, N. Bischof, W. Tiereth, I. Weitzenfelder, W. von Oertzen, and B. Imanishi, Nucl. Phys. **A476**, 491 (1988).
[10] E. Liénard, D. Baye, Th. Delbar, P. Descouvemont, P. Duhamel, W. Galster, M. Kurokawa, P. Leleux, I. Licot, P. Lipnik, C. Michotte, T. Motobayashi, A. Ninane, J. Vanhorenbeeck, and J. Vervier, in Proceedings of the Fifth International Conference on Nucleus-Nucleus Collisions, Taormina, 1994 [Nucl. Phys. **A583**, 783 (1995)].
[11] W. von Oertzen and H.G. Bohlen, Phys. Rep. **19C**, 1 (1975).
[12] B. Imanishi and W. von Oertzen, Phys. Rep. **155**, 29 (1987).
[13] D. Baye, J. Deenen, and Y. Salmon, Nucl. Phys. **A289**, 511 (1977).
[14] D. Baye, Nucl. Phys. **A460**, 581 (1986).

[15] D. Baye and P. Descouvemont, Nucl. Phys. **A507**, 497 (1990).
[16] A. Adahchour, D. Baye, and P. Descouvemont, Nucl. Phys. **A579**, 305 (1994).
[17] M. Kurokawa, T. Motobayashi, K. Ieki, S. Shimoura, H. Murakami, Y. Ikeda, S. Moriya, Y. Yanagisawa, and T. Nomura, IEEE Trans. Nucl. Sci. **42**, 192 (1995).
[18] S. Trentalange, S.-C. Wu, J.L. Osborne, and C.A. Barnes, Nucl. Phys. **A483**, 406 (1988).
[19] F. James and M. Ross, CERN Report No. D506, 1983.
[20] D. Baye, Nucl. Phys. **A272**, 445 (1976).
[21] P.J.A. Buttle and L.J.B. Goldfarb, Nucl. Phys. **78**, 409 (1966).
[22] H.P. Gubler, G.R. Plattner, I. Sick, A. Traber, and W. Weiss, Nucl. Phys. **A284**, 114 (1977).
[23] F.C. Barker and N. Ferdous, Aust. J. Phys. **33**, 691 (1980).
[24] J. Cook, M.N. Stephens, K.W. Kemper, and A.K. Abdallah, Phys. Rev. C **33**, 915 (1986).
[25] A. Richter and C. Toepffer, in *Heavy Ion Collisions*, edited by R. Bock (North-Holland, Amsterdam, 1979), Vol. 1, p. 1.
[26] P.J.A. Buttle and L.J.B. Goldfarb, Nucl. Phys. **A115**, 461 (1968).